Supporting Information

In-Situ Synthesis of Conductive Porous $Ni_{1.5}Cu_{1.5}(HHTP)_2$ on Carbon Paper for Enhanced Rechargeable Li-O_2 Batteries

Si Miao [a], Pingan Pan [a], Ying Zhang [a], Shilin Huo [a], Doufeng Wu [a, *], and Sanchuan Yu [a, *]

[a] School of Chemistry and Chemical Engineering, Zhejiang Sci-Tech University, Hangzhou 310018, People's Republic of China

* Corresponding author: Zhejiang Sci-Tech University, School of Chemistry and Chemical Engineering, Hangzhou 310018, People's Republic of China.

Tel.: +86-571-86843217; Fax: +86-571-86843217.

E-mail: dfwu@zstu.edu.cn (D. Wu), yuschn@163.com (S. Yu).

1. Experimental section

Preparation of CP-OH, $M_3(HHTP)_2$/CP, $Ni_xCu_{3-x}(HHTP)_2$/CP

CP-*OH*: The CP was cut into discs with a diameter of 16 mm. These were then soaked in deionised water for a period of 30 minutes, followed by a further 30 minutes in ethanol. Finally, they were dried at a temperature of 60 °C. A solution of 100 mL deionized water was prepared in a beaker, and the pH was adjusted to 4 with 0.1 mol L^{-1} hydrochloric acid. Subsequently, 1 g of $FeCl_2 \cdot 4H_2O$ was added, and the CP was introduced to the beaker after thorough stirring and dissolution. The mixed solution ($V_{30\ \%\ H2O2}$: $V_{\text{deionized water}}$ =1 : 3) was injected at a rate of 50 mL h^{-1} at 35 °C for 2 h. Subsequently, the carbon paper was washed with 0.1 mol L^{-1} hydrochloric acid in order to remove the residual Fe^{3+} on its surface. Subsequently, the material should be washed with deionised water until the pH is neutralised. It should then be subjected to vacuum drying at 60 °C for 12 hours, with the weight of the material recorded.

$M_3(HHTP)_2$/CP: *The synthesis of $Ni_3(HHTP)_2$/CP*: $Ni(CH_3COO)_2 \cdot 4H_2O$ (18.66 mg, 0.075 mmol) and 5 mL deionized water were added to a 20 mL glass bottle and ultrasonicated for 10 min. After the metal salt was completely dissolved, CP was put into the solution and stood for 1 h to form solution A. Another 20 mL glass bottle was added with ligand HHTP (16.26 mg, 0.05 mmol) and 5 mL deionized water, and the solution B was formed by ultrasonication for 20 min. The solution A was poured into solution B, and 1.25 mL DMF was added. The glass bottle was placed in a constant temperature oven at 85 °C for 24 h. After natural cooling to room temperature, CP was washed three times with 5 mL deionized water and 5 mL acetone, and finally dried in a vacuum oven at 60 °C for 12 h. The mass of the active substance was calculated by the difference method.

$Cu_3(HHTP)_2$/CP: $Cu(CH_3COO)_2 \cdot H_2O$ (14.85 mg, 0.075 mmol), HHTP (16.26 mg, 0.05 mmol), the preparation method is consistent with $Cu_3(HHTP)_2$/CP.

$Ni_xCu_{3-x}(HHTP)_2$/CP: $Ni(CH_3COO)_2·4H_2O$ (12.44 mg, 0.05 mmol), $Cu(CH_3COO)_2·H_2O$ (9.98 mg, 0.05 mmol) and 5 mL deionized water were added to a 20 mL glass bottle. The ratio of $Ni(CH_3COO)_2·4H_2O$ to $Cu(CH_3COO)_2·H_2O$ was 1 : 1, and the mixture was sonicated for 10 min. CP was placed in the mixed solution and allowed to stand for 1 h to form solution A. Another 20 mL glass bottle was added with HHTP (21.6 mg, 0.067 mmol) and 5 mL deionized water, and the solution B was formed by ultrasonication for 20 min. The solution A was poured into solution B, and 1.25 mL DMF was added. The glass bottle was placed in a constant temperature oven at 85 °C for 24 h. After natural cooling to room temperature, CP was washed three times with 5 mL deionized water and 5 mL acetone, and finally dried in a vacuum oven at 60 °C for 12 h. The mass of the active substance was calculated by the difference method. $Ni_{2.25}Cu_{0.75}(HHTP)_2$/CP (the ratio of $Ni(CH_3COO)_2·4H_2O$ and $Cu(CH_3COO)_2·H_2O$ is 1 : 3) and $Ni_{0.75}Cu_{2.25}(HHTP)_2$ (the ratio of $Ni(CH_3COO)_2·4H_2O$ and $Cu(CH_3COO)_2·H_2O$ is 3 : 1) were prepared by the same method.

Materials characterization： Its morphology and element distribution were characterized by scanning electron microscopy (SEM, Hitachi SU8100). The crystal phase of powders and electrodes was examined by X-ray diffraction (XRD, Bruker AXS GmbH, Copper Kα, λ=1.54178 Å) in the 2θ range of 2.0-50.0° at the scan rate of 2.4° min^{-1} in steps of 0.02°. Elemental content analysis of materials was measured by inductively coupled plasma optical emission spectrometry (ICP-OES) after appropriate dilution. Nitrogen adsorption and desorption method (Micrometrics Corporation, ASAP 3020, 77K) was used to obtain the specific surface area and pore size distribution of the samples by BET and BJH methods, respectively. The AC electrochemical impedance of the battery was determined by the electrochemical workstation (CHI604E).

Preparation of cathode material： The cathodes were prepared by casting a slurry of the material on a hydrophobic carbon paper. The slurry consisted of 80 wt%

synthesized materials as the catalyst and 20 wt% polyvinylidene fluoride dispersed in 1-methyl-2-pyrrolidone. The casted cathodes were dried in an 80 °C vacuum oven for 24 h.

Electrochemical measurements: The battery was assembled in a glove box filled with pure argon. Li/separator (Celgard 2400) (dipped with electrolyte)/O_2 electrode was sealed into a Swagelok cell with an air hole placed on the positive electrode side to allow the oxygen to flow in. A Swagelok cell was assembled with three layers separator (Celgard 2400), a lithium foil anode (thickness, 500 μm), and 400 μL of 1.0 M bis(trifluoromethane) sulfonamide lithium salt (LiTFSI) in tetraethylene glycol dimethyl ether electrolyte. After assembly, the batteries were stabilized in a pure oxygen atmosphere for 6 h at room temperature. All the cell performance evaluations were based on the weight of synthesized materials with a total loading of 0.7-1.2 mg. The full charge-discharge profiles of Li-O_2 cells were tested in the voltage window from 2.0 to 4.5 V and at a rate of 500 mA g^{-1} in a LAND cycler (Wuhan Land Electronic Co. Ltd). The cycling test was conducted at a specific capacity limit of 500 mAh g^{-1} at a current density of 50 mA g^{-1}. Electrochemical impedance spectroscopy (EIS) was measured at an AC voltage of 5 mV amplitude in the frequency range between 0.01 Hz and 10^5 Hz.

2. Results and discussion

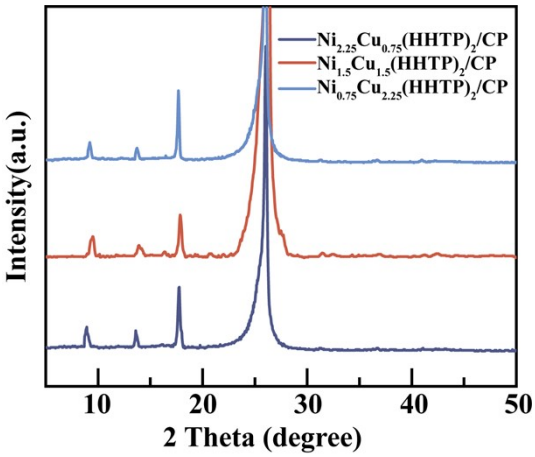

Fig. S1 X-ray diffraction (XRD) diagram of $Ni_{2.25}Cu_{0.75}(HHTP)_2$/CP, $Ni_{1.5}Cu_{1.5}(HHTP)_2$/CP and $Ni_{0.75}Cu_{2.25}(HHTP)_2$/CP

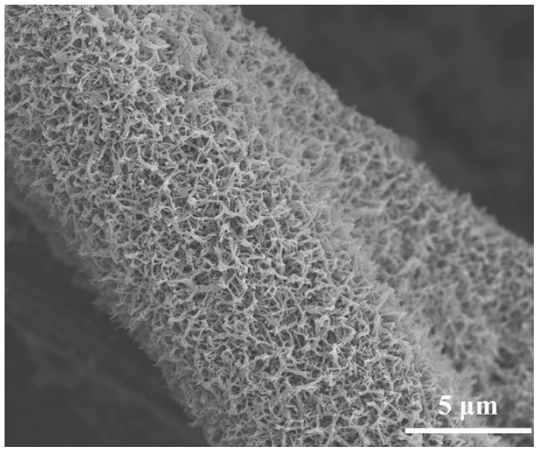

Fig. S2 SEM images of the $Ni_3(HHTP)_2$/CP cathodes

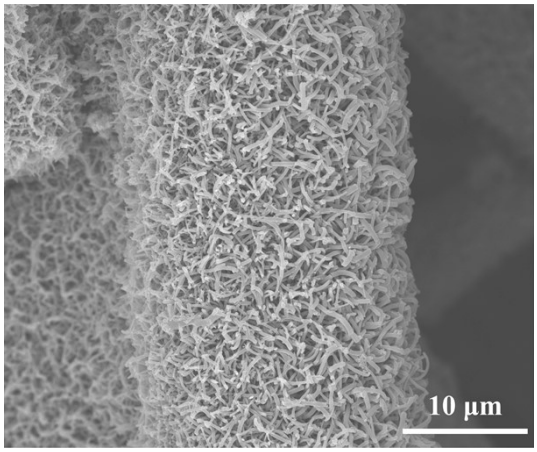

Fig. S3 SEM images of the $Cu_3(HHTP)_2$/CP cathodes

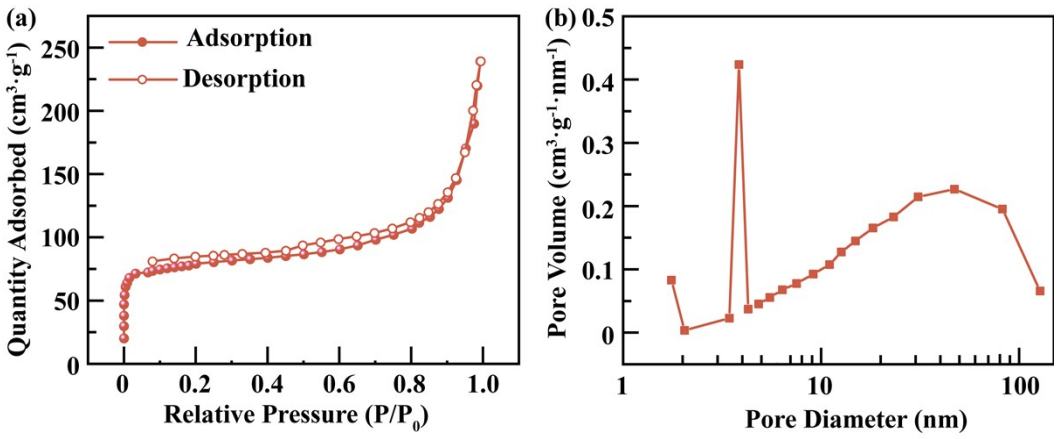

Fig. S4 N_2 adsorption/desorption isotherm (a) and pore size distribution (b) of $Ni_{1.5}Cu_{1.5}(HHTP)_2$/CP

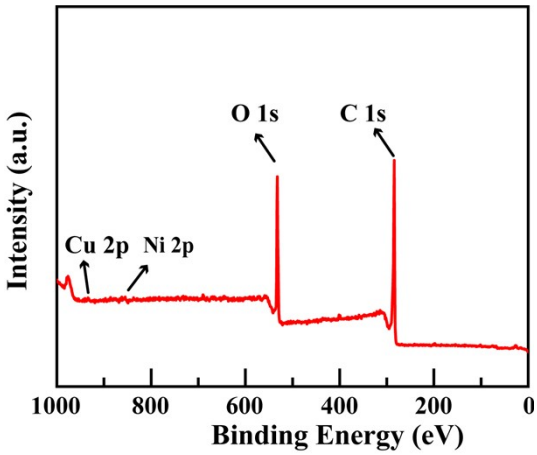

Fig. S5 XPS survey of $Ni_{1.5}Cu_{1.5}(HHTP)_2$/CP

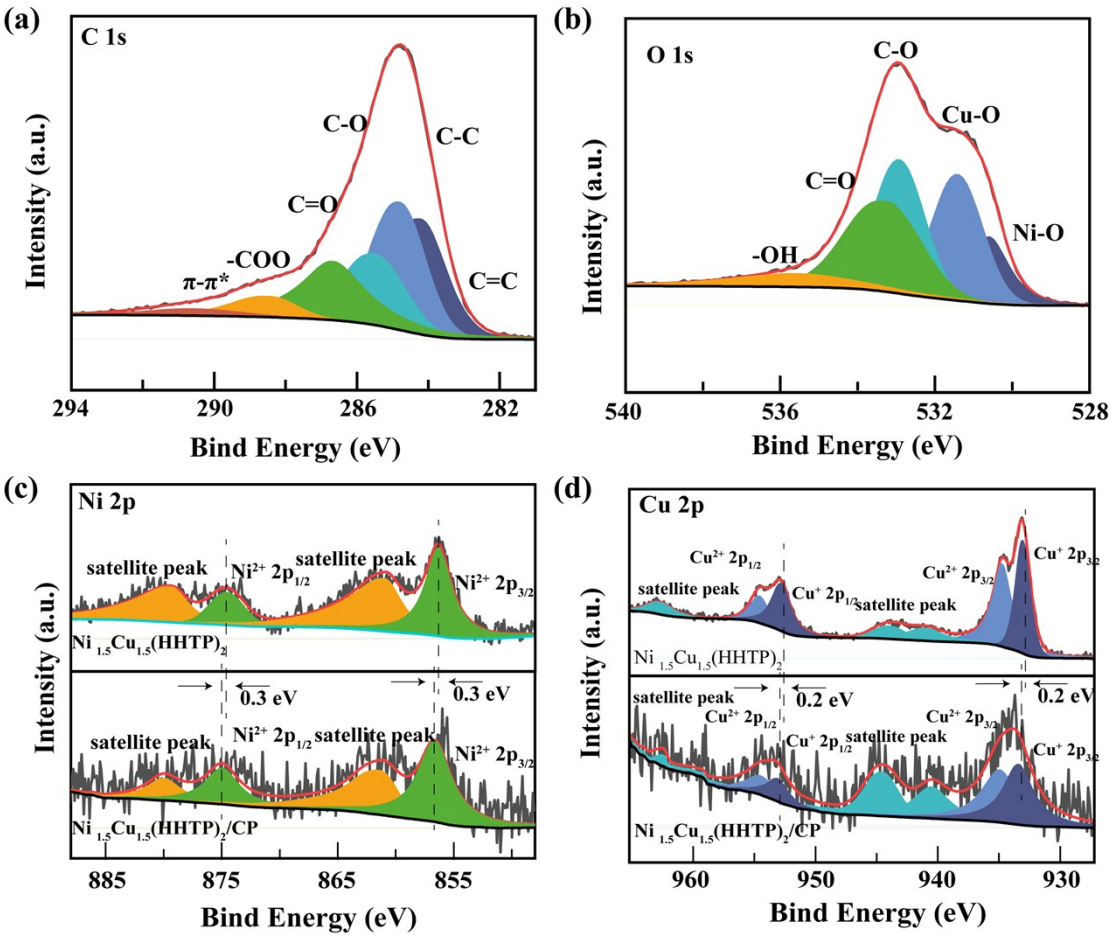

Fig. S6 (a) O 1s high-resolution mapping of $Ni_{1.5}Cu_{1.5}(HHTP)_2$/CP, (b) C 1s high-resolution mapping of $Ni_{1.5}Cu_{1.5}(HHTP)_2$/CP, (c) Ni 2p high-resolution mapping of $Ni_{1.5}Cu_{1.5}(HHTP)_2$ and $Ni_{1.5}Cu_{1.5}(HHTP)_2$/CP, (d) Cu 2p high-resolution mapping of $Ni_{1.5}Cu_{1.5}(HHTP)_2$ and $Ni_{1.5}Cu_{1.5}(HHTP)_2$/CP

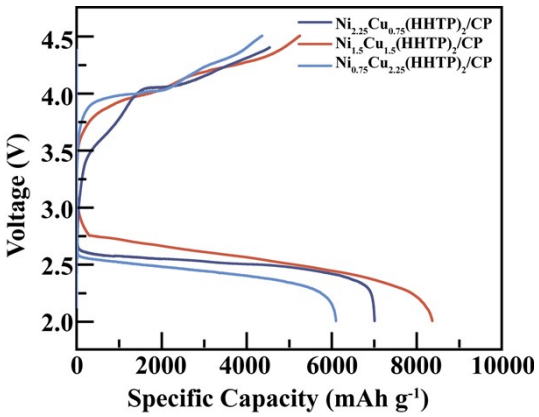

Fig. S7 Galvanostatic full discharge and recharge profiles of $Ni_{2.25}Cu_{0.75}(HHTP)_2$/CP, $Ni_{1.5}Cu_{1.5}(HHTP)_2$/CP and $Ni_{0.75}Cu_{2.25}(HHTP)_2$/CP electrodes at current density of 50 mA g^{-1}

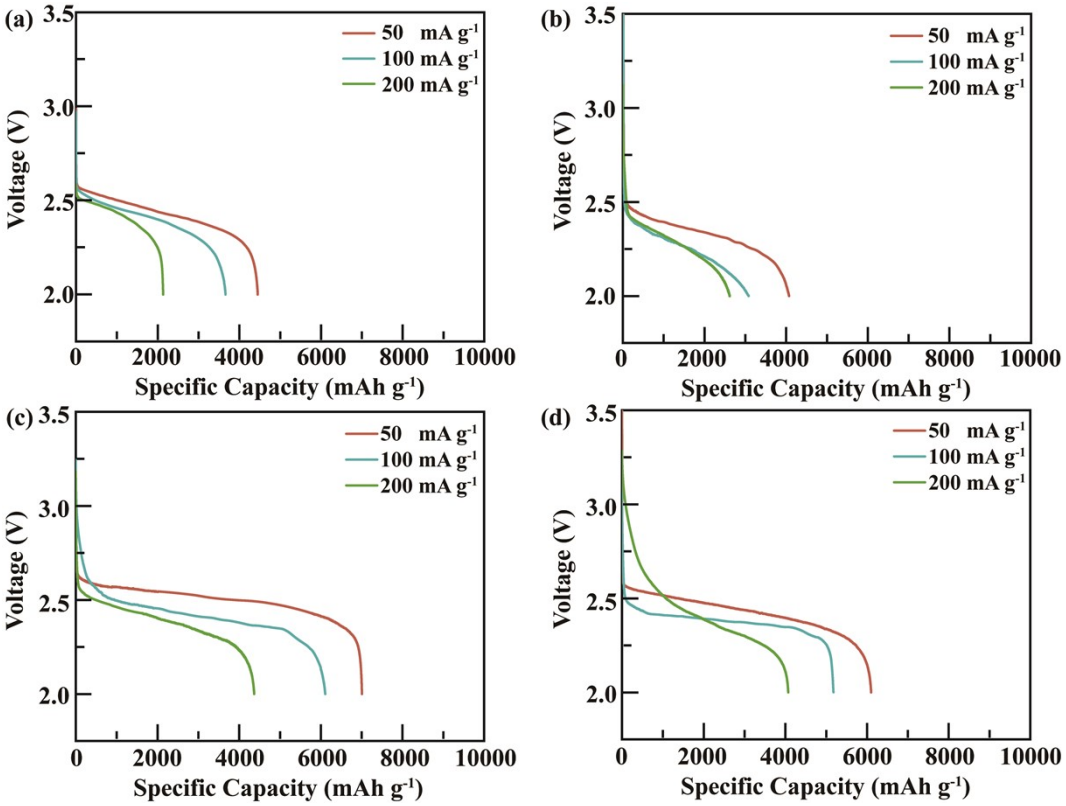

Fig. S8 Discharge/charge curves of (a) $Ni_3(HHTP)_2$/CP, (b) $Cu_3(HHTP)_2$/CP, (c) $Ni_{2.25}Cu_{0.75}(HHTP)_2$/CP and (d) $Ni_{0.75}Cu_{2.25}(HHTP)_2$/CP cathode at different current densities

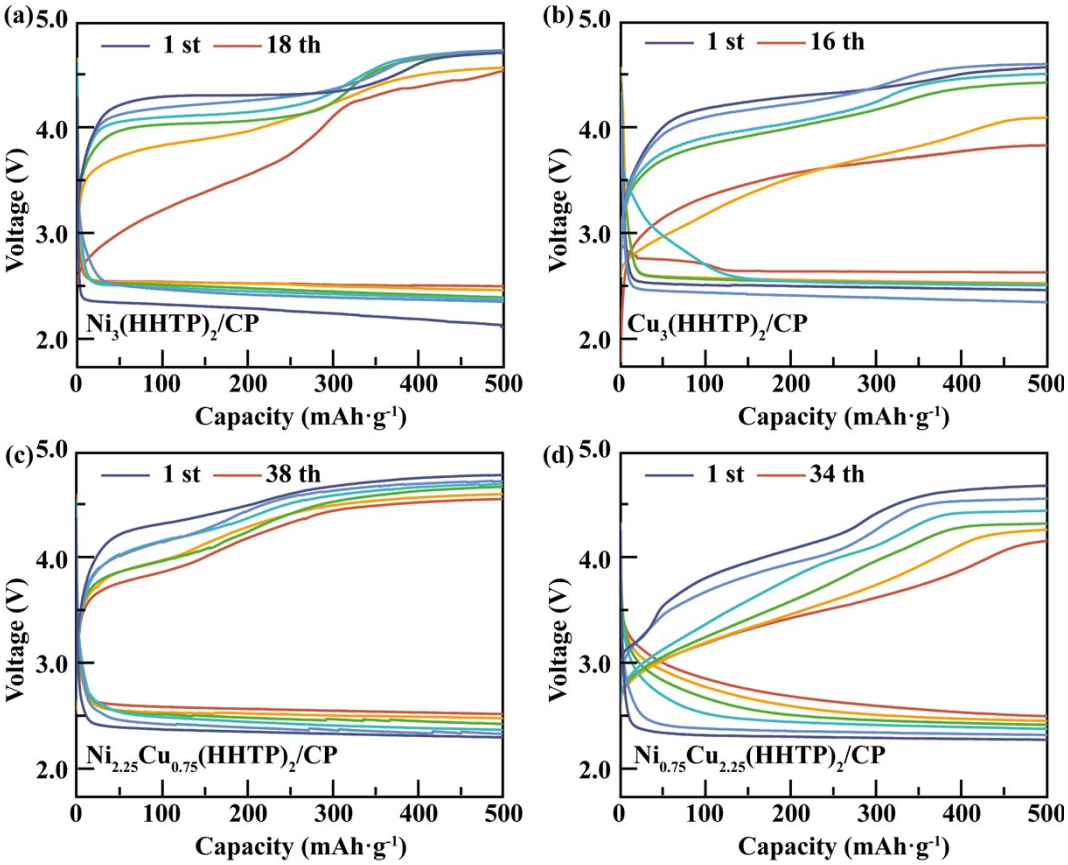

Fig. S9 The cycle stability of the (a) $Ni_3(HHTP)_2$/CP, (b) $Cu_3(HHTP)_2$/CP, (c) $Ni_{2.25}Cu_{0.75}(HHTP)_2$/CP and (d) $Ni_{0.75}Cu_{2.25}(HHTP)_2$/CP electrodes based on Li-O_2 batteries

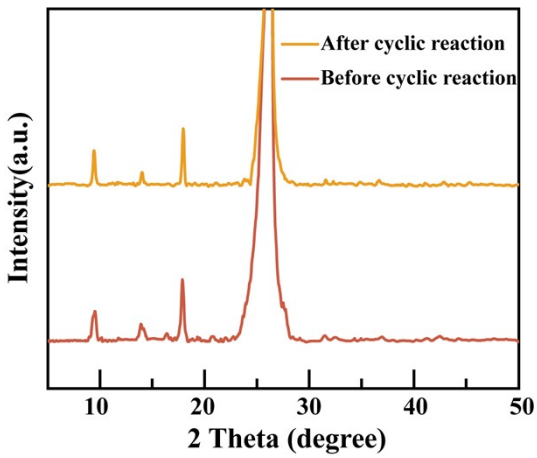

Fig. S10 The XRD patterns of the $Ni_{1.5}Cu_{1.5}(HHTP)_2$/CP before and after cyclic reaction

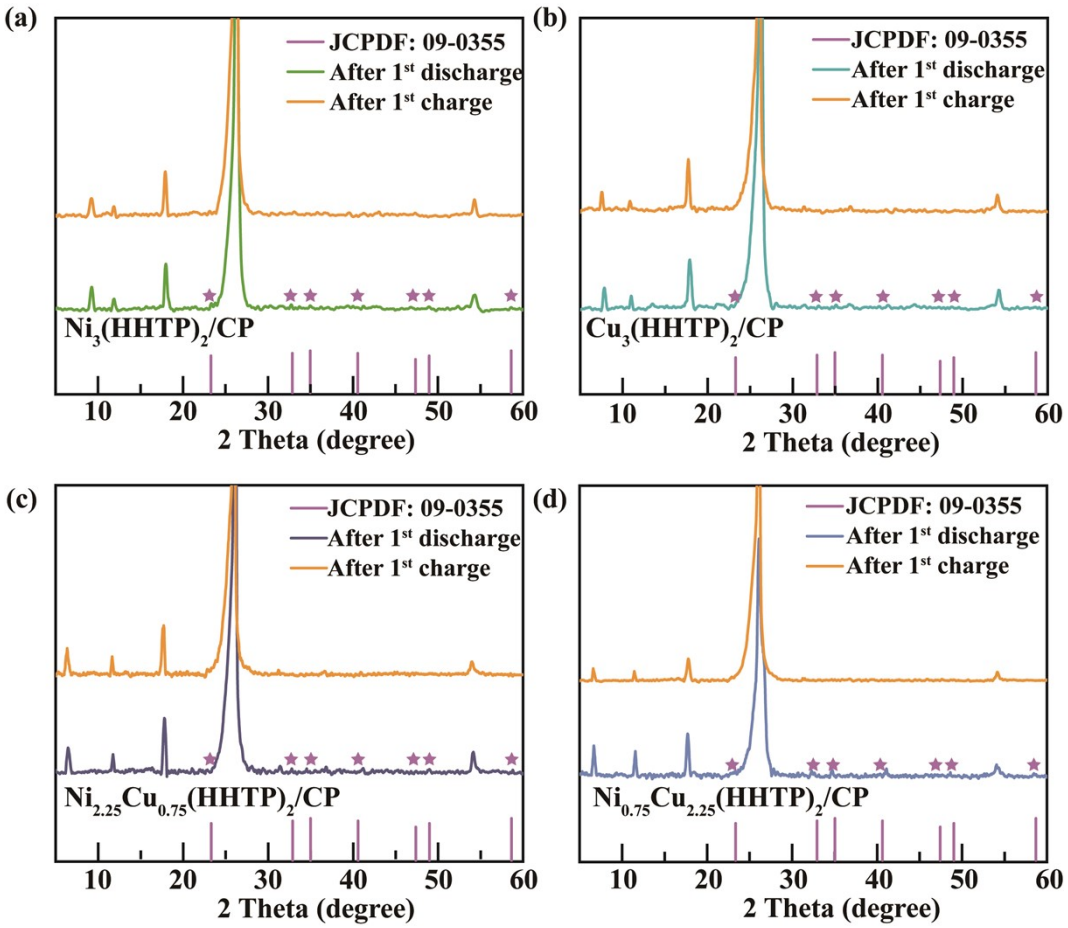

Fig. S11 The ex-situ XRD patterns of the (a) $Ni_3(HHTP)_2$/CP, (b) $Cu_3(HHTP)_2$/CP, (c) $Ni_{2.25}Cu_{0.75}(HHTP)_2$/CP and (d) $Ni_{0.75}Cu_{2.25}(HHTP)_2$/CP based electrodes at pristine, discharged and recharged states

Table S1 ICP test results of $Ni_xCu_{3-x}(HHTP)_2$/CP

Sample	Cu (theoretical ratio %)	Cu (actual ratio %)	Ni (theoretical ratio %)	Ni (actual ratio %)
$Ni_{2.25}Cu_{0.75}(HHTP)_2$/CP	25.0	16.5	75.0	83.5
$Ni_{1.5}Cu_{1.5}(HHTP)_2$/CP	50.0	75.9	50.0	24.1
$Ni_{0.75}Cu_{2.25}(HHTP)_2$/CP	75.0	84.8	25.0	15.2

Table S2 Fitted impedance parameters of the Li-O_2 battery with different cathode

Sample	$R_{ct}(\Omega)$
CP	204.833
$Ni_3(HHTP)_2$/CP	104.241
$Cu_3(HHTP)_2$/CP	114.136
$Ni_{2.25}Cu_{0.75}(HHTP)_2$/CP	72.412
$Ni_{1.5}Cu_{1.5}(HHTP)_2$/CP	61.286
$Ni_{0.75}Cu_{2.25}(HHTP)_2$/CP	66.348

Table S3 Performance comparison of Li-O_2 batteries with different oxygen electrodes

Oxygen electrodes	**Specific capacity (mAh g^{-1})**	**Cycle stability (Cycles)**	**Reference**
$Ni_{1.5}Cu_{1.5}(HHTP)_2$/CP	8367 (50 mA g^{-1})	43 (50 mA g^{-1})	This work
MoO_2 supported Mo_3P@Mo	4720 (500 mA g^{-1})	500 (500 mA g^{-1})	1
$NiCo_2O_4$@CeO_2	5586 (500 mA g^{-1})	400 (500 mA g^{-1})	2
Co_3O_4-H	5220 (200 mA g^{-1})	120 (200 mA g^{-1})	3
N, Co-TiO_2/CFs	5300 (100 mA g^{-1})	50 (200 mA g^{-1})	4
CNS-RAs/CT	5438 (500 mA g^{-1})	588 (300 mA g^{-1})	5
CuO-$CuCo_2O_4$	6844 (100 mA g^{-1})	130 (400 mA g^{-1})	6
Co_9S_8-PCF	6875 (50 mA g^{-1})	105 (100 mA g^{-1})	7
Mn-MOF	5579	140	8

	(0.2 mA cm^{-2})	(0.2 mA cm^{-2})	
Dy-BTC	7618 (50 mA g^{-1})	76 (200 mA g^{-1})	9
Tz-Mg-MOF-74	7700 (50 mA g^{-1})	28 (200 mA g^{-1})	10

References

[1] T. Yang, Y. Xia, T. Mao, Q. Ding, Z. Wang, Z. Hong, J. Han, D.-L. Peng and G. Yue, *Adv. Funct. Mater.*, 2022, **32**, 2209876

[2] Y. Wu, H. Ding, T. Yang, Y. Xia, H. Zheng, Q. Wei, Han, Jiajia, D.-L. Peng and G. Yue, *Advanced Science*, 2022, **9**, 2200523.

[3] Y. Zheng, R. Gao, L. Zheng, L. Sun, Z. Hu and X. Liu, *ACS Catal.*, 2019, **9**, 3773-3782.

[4] W.-L. Bai, S.-M. Xu, C.-Y. Xu, Q. Zhang, H.-H. Wang, Z. Zhang, X. Chen, S.-Y. Dong, Y.-S. Liu, Z.-X. Xu, X.-G. Zhang, Z. Wang, K.-X. Wang and J.-S. Chen, *J. Mater. Chem. A*, 2019, **7**, 23046-23054.

[5] A. Hu, J. Long, C. Shu, C. Xu, T. Yang, R. Liang and J. Li, *Electrochim. Acta*, 2019, **301**, 69-79.

[6] S.-y. Zhen, H.-t. Wu, Y. Wang, N. Li, H.-s. Chen, W.-l. Song, Z.-h. Wang, W. Sun and K.-n. Sun, *RSC Adv.*, 2019, **9**, 16288-16295.

[7] X. Lin, R. Yuan, S. Cai, Y. Jiang, J. Lei, S.-G. Liu, Q.-H. Wu, H.-G. Liao, M. Zheng and Q. Dong, *Adv. Energy Mater.*, 2018, **8**, 1800089.

[8] S. Yu, H. Zhao, Y. Wang, X. Lang, T. Wang, T. Qu, L. Li, C. Yao and K. Cai, *Appl. Organomet. Chem.*, 2024, **38**, e7658.

[9] D. Liu, X. Zhang, Y.-J. Wang, S. Song, L. Cui, H. Fan, X. Qiao and B. Fang, *Nanoscale*, 2020, **12**, 9524-9532.

[10] N. Li, Z. Chang, M. Zhong, Z.-X. Fu, J. Luo, Y.-F. Zhao, G.-B. Li and X.-H. Bu, *CCS Chem.*, 2021, **3**, 1297-1305.